139 (2022) 213013

Contents lists available at ScienceDirect

Biomaterials Advances

journal homepage: www.journals.elsevier.com/materials-science-and-engineering-c

The anticancer properties of metal-organic frameworks and their heterogeneous nanocomposites

Yashar Rezaeipour [a,1], Ehsan Zolghadr [b,1], Parvin Alizadeh [a,*], Ghazal Sadri [c], Evan K. Wujcik [d], Farhad Akbari Afkhami [e], Mark Elliott [b,*], Mostafa Dadashi Firouzjaei [b,*]

[a] Department of Materials Science and Engineering, Faculty of Engineering & Technology, Tarbiat Modares University, P. O. Box: 14115-143, Tehran, Iran
[b] Department of Civil, Construction and Environmental Engineering, University of Alabama, Tuscaloosa, AL 35487, USA
[c] Department of Biochemistry and Molecular Genetics, University of Louisville, Louisville, KY 40292, USA
[d] Department of Chemical and Biological Engineering, University of Alabama, Tuscaloosa, AL, 35487, USA
[e] Department of Chemistry and Biochemistry, University of Alabama, Tuscaloosa, AL, 35487, USA

ARTICLE INFO

Keywords:
MOF
cancer
bacteria
Green engineering
cancer treatment
Nanotechnology
Metal-organic framework

ABSTRACT

Herein, silver-based metal-organic framework (AgMOF) and its graphene oxide (GO)-decorated nanocomposite (GO-AgMOF) are proposed for use in emerging biomedical applications. The nanocomposites are characterized, and hence, in vitro apoptotic and antibacterial features of AgMOF and GO-AgMOF nanomaterials were investigated. An MTT cytocompatibility assay indicates that these nanomaterials have dose-dependent toxicity in contact with SW480, colon adenocarcinoma cells. In addition, the cell death mechanism was explored by analyzing flow cytometry and caspase activity. Furthermore, the expressions of pro-apoptotic and anti-apoptotic genes were investigated using quantitative polymerase chain reaction (qPCR). Comparing the control group with the groups treated by the nanomaterials indicates up-regulation of the BAX/BCl2 ratio. We also measured the minimum inhibitory concentration (MIC) and minimum bacterial concentration (MBC) of these nanomaterials acting on *S. mutans* and *S. aureus*, which indicates excellent antibacterial properties. Showing inhibition effect on the viability of cancerous cells through apoptosis and antibacterial effects simultaneously, AgMOF and GO-AgMOF can be regarded as potential therapeutics for cancer.

1. Introduction

As the leading cause of death worldwide, cancer is expected to cause 13.1 million annual deaths by 2030 [1,2]. Rapid and uncontrolled cell differentiation is the main characteristic of cancer that causes immature vascular systems in tumor tissues due to slow vascularization [3]. Cancer causes mortality by different mechanisms, i.e., infection, hemorrhage, and neoplastic extension [4]. There are several methods for treating cancer, including deoxyribonucleic acid (DNA) targeting [5], interfering with DNA synthesis [6] and preventing cell replication [7] by chemotherapy [8], puncturing DNA by radiotherapy [9], and tumor resection. However, the available therapeutic approaches withal lead to adverse side effects such as gastritis, fatigue, and bleeding in organs [9–11]. Therefore, developing new therapies with fewer side effects is required for a better cancer prognosis [12].

Different studies have shown that various nanomaterials including gold [13], silver [14], and cerium oxide [15], can be effective anticancer agents [16]. These nanomaterials' unique characteristics, including high surface area, in addition to tunable optical, electrical, and magnetic properties, have yielded promising applications in clinical trials over the last 20 years [17–19]. There are diverse mechanisms by which nanomaterials are used for cancer therapy. For instance, some mechanisms are based on nanomaterials redox activity which has biological effects on the tumor [20]. Some others are under the interaction of nanomaterials with the human immune system [21,22]; for example, Jia et al. [23] have shown that targeting dendritic cells by nanomaterials could be a promising strategy for cancer therapy. However, one of the challenges regarding cancer therapy is the interference of bacteria in cancer cell development and treatment [1]. It has been indicated that some bacteria can mediate and exacerbate cancer by thriving inside cancerous tissues [24,25]. In addition, microbial infections would diminish the therapeutic efficacy during the treatment and lead to

* Corresponding author.
E-mail addresses: p-alizadeh@modares.ac.ir (P. Alizadeh), melliott@eng.ua.edu (M. Elliott), mdfirouzjaei@crimson.ua.edu (M. Dadashi Firouzjaei).
[1] Authors contributed equally to this work

https://doi.org/10.1016/j.bioadv.2022.213013
Received 12 February 2022; Received in revised form 3 June 2022; Accepted 30 June 2022
Available online 5 July 2022

severe difficulties [1,26,27]. Therefore, using nanomaterials with antibacterial properties in cancer treatment is essential [28,29].

Metal-Organic Frameworks (MOFs) are synthetic nanoporous hybrid materials made of metal cores and organic cross-linkers [30,31]. MOFs have been scaled down to nano-metric structures, and they combine the benefits of porous materials and nanostructures [32]. Silver nanomaterials (Ag-Nanomaterials) as one of the metallic cores of MOFs show antibacterial [33], antiviral [34], and anticancer behavior [14]. Ag-nanomaterials have been previously applied for treating breast cancer [35]. However, all traditional carriers suffer from different restrictions in bio-applications [36]; for example, micelles and liposomes have low loading capacities [37], and inorganic porous materials suffer from unacceptable degradability and undesirable toxicity [38]. On the other side, MOFs possess several advantages; first, due to their tunable structures, MOFs could have diverse morphologies, sizes, compositions, and chemical properties, which provide them with multi-functionalities [39]; second, MOFs possess high loading capacity owning to their large surface area and high porosity [36]; third, MOFs are bio-degradable because of weak coordination bonds [36].

Despite MOFs' excellent properties and approving applications, there is still room to improve their biomedical properties by incorporating additives into their structure. Graphene oxide (GO) is a derivative of graphene [40] that can hinder MOF aggregation [41], enlarge the surface area, and enhance its dispersion [42]. Moreover, previous studies have shown that GO inhibits cancer cells' migration and tumor growth [43]. Another critical parameter that makes GO an attractive candidate in biomedical applications is its high aspect ratio due to its 2D structure, which causes more interaction with the biological system [44]. Considering what was stated above, it can be concluded that GO is one of the most suitable materials that can be added to the MOF-based composites [45] to improve biomedical properties. Therefore, here in this study, a previously described novel silver MOF (AgMOF), embellished with GO, denoted as GO-AgMOF [46], has been investigated for the possibility of its application as an anticancer drug.

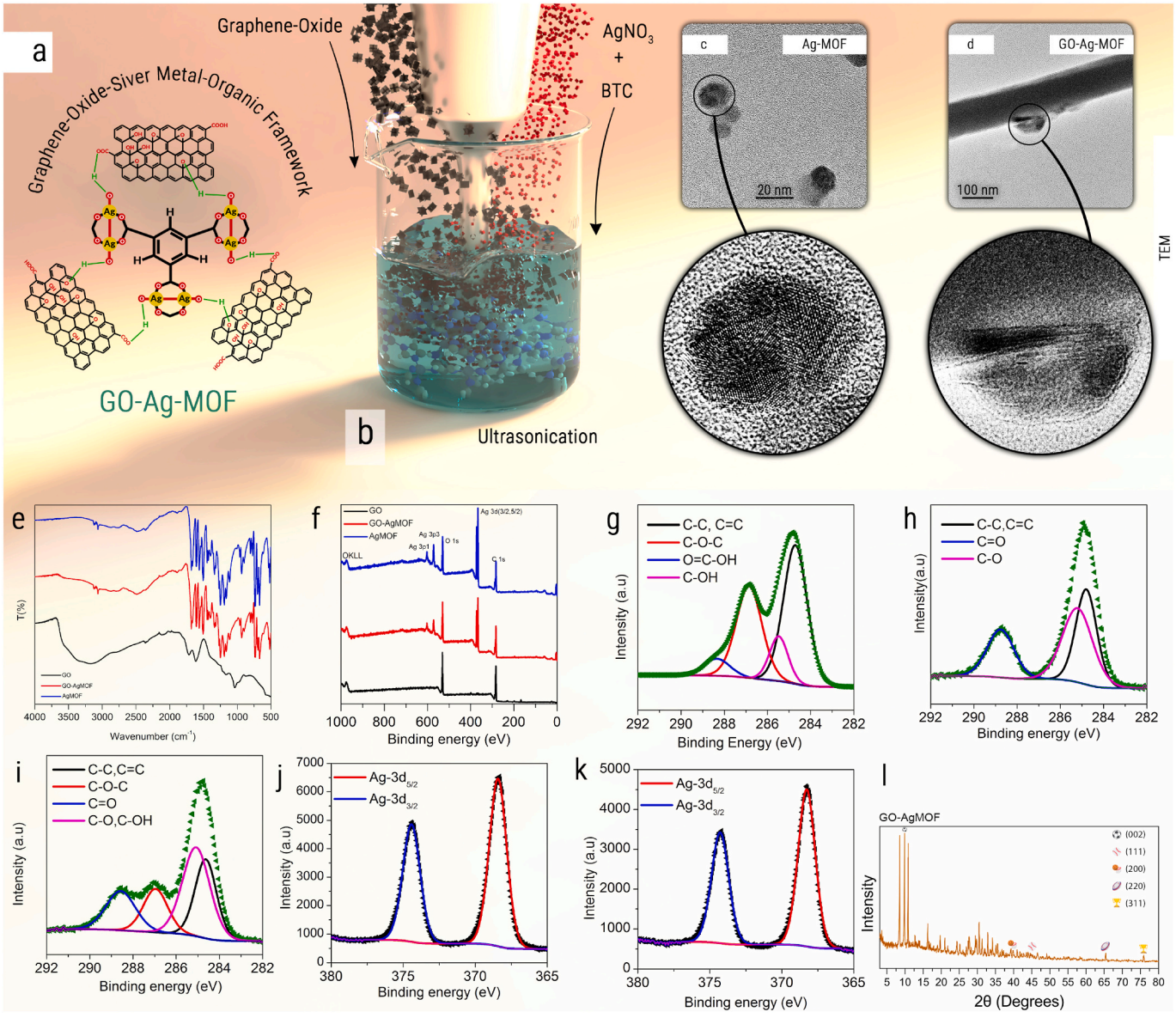

Fig. 1. (a) The chemical structure of GO-AgMOF. (b) The schematic illustration of the GO-AgMOF synthesis process. TEM images of (c) AgMOF and (d) GO-AgMOF nanomaterials. (e) FTIR spectra of GO, AgMOF, and GO-AgMOF nanoparticles. (f) The XPS spectra of GO, AgMOF, and GO-AgMOF; the high resolution spectrum of C 1 s is shown for (g) GO, (h) AgMOF, and (i) GO-AgMOF; the high resolution spectrum of Ag 3d is shown for (j) AgMOF and (k) GO-AgMOF. (l) The XRD pattern of GO-AgMOF.

2. Materials and methods

2.1. Reagents

Silver nitrate ($AgNO_3$), 3-(4,5-dimethylthiazol-2-yl)-2,5-diphenyltetrazolium bromide (MTT), dimethyl sulfoxide (DMSO), dithiothreitol (DTT), Mueller Hinton broth (M-H broth), and benzene-1,3,5-tricarboxylic acid (BTC) have been purchased from Merck, Germany. Caspase-3, −8, and − 9 activity kits were supplied from Abnova, Thailand. Fluorescein isothiocyanate (FITC)-conjugated Annexin V and propidium iodide (FITC-Annexin-V/PI) staining kit was from Hoffman-La Roch Ltd. Switzerland, and RNeasy Plus Mini Kit was from Qiagen, Germany. cDNA Synthesis Kit was acquired from Prime Script, Japan. ABI 7300 real-time PCR (also known as quantitative PCR or qPCR) system was from Applied Biosystems, USA. Ethanol (99.7 %) was purchased from US VWR, and GO (US7906) was provided by U.S. Research Nanomaterial Inc.

2.2. Nanomaterials fabrication, characterization, and toxicity tests

AgMOF and GO-AgMOF were synthesized based on the method described by Firouzjaei et al. [46]. First, to synthesize GO-AgMOF, 0.5 g of BTC in 20 mL of ethanol and 0.5 g of silver nitrate in 20 mL of water were dissolved for 30 min. In the next step, 50 mg of GO powder was added to the solution and was sonicated for 1 h using an ultrasonic probe with 0.5 pulses, 40 W output energy, and 20 kHz frequency (QSonica, Newtown, Connecticut, USA). The solution was dried in the oven for 24 h at 40 °C. For synthesizing AgMOF, the exact sonication process was carried out except for the addition of GO in the solution. The schematic illustration of the fabrication process and chemical formula of GO-AgMOF are depicted in Fig. 1. Silver nanoparticles were fabricated to compare the properties of MOFs with other types of nanostructures. In brief, 5 mL of sodium citrate 0.05 M (TSC, SigmaAldrich) and 5 mL of silver nitrate 0.05 M were added to 185 mL of distilled water in a cold bath between 6 °C to 10 °C. The solution was stirred at 3000 rpm for 3 min. After that, 5 mL of sodium borohydride 0.05 M (NaBH4, Sigma-Aldrich) was dripped slowly. The pH was adjusted to 10 using 1.25 M sodium hydroxide (NaOH, PANREAC). The nanoparticles obtained and kept in amber bottles at 4 °C. Transmission electron microscopy (TEM, FEI Tecnai F-20) was used for physical characterization of nanoparticles. Attenuated total reflection–Fourier transform infrared (ATR-FTIR; Varian Excalibur FTS-3000) spectroscopy was employed to study the functional groups of the nanomaterials. Furthermore, the crystalline structures were probed using X-ray powder diffraction (XRD; XPERT-PRO). In addition, the X-ray photoelectron spectroscopy (XPS; Bestec, Germany) equipped with a 100-micron monochromatic Al Kα X-ray source was utilized to identify the elemental compositions. Dynamic light scattering (DLS; Nano ZS ZEN 3600) was applied to determine the size of the nanoparticles. In this process, the samples with half molar concentration were initially stabilized in water via sonication. Thus, the volume, intensity, and number of peaks were taken into account to identify the size distribution. Furthermore, a UV–Vis spectrophotometer (PerkinElmer LAMBDA 35) was used to acquire the absorption spectra.

Furthermore, the toxicity of the nanomaterials was evaluated by using an MTT assay. The cell death mechanism was investigated by quantitative polymerase chain reaction (qPCR), flow cytometry, and caspase activity. Moreover, the nuclei fragmentation was determined by Hoechst staining. In addition, *S. mutans* and *S. aureus* bacteria were used to investigate the antibacterial properties of the nanomaterials (discussion regarding antibacterial properties of materials can be found in supporting information).

2.3. MTT assay test

The first step in evaluating the nanomaterials as a potential candidate for cancer treatment is to investigate their cytocompatibility. This step was taken by using an MTT assay. Briefly, 1×10^4 cells were seeded in each well of 96-well tissue culture grade plates and incubated at 37 °C with 5 % atmospheric CO_2 for one day. Cells were then treated with several concentrations of nanomaterials in a decreasing manner (50 down to 0.78 μg/mL for both AgMOF and GO-AgMOF, and 500 down to 7.81 μg/mL for GO). Next, 100 μL of MTT solution was added to each well. After 4 h of incubation, 100 μL of DMSO was added to each well to solve formed formazan crystals. At the end, formazan absorbance was measured at 570 nm.

2.4. Flow cytometry test

FITC-Annexin-V/PI staining kit was used as the cytotoxicity marker to determine the apoptosis of cells. The rates of cell apoptosis were measured utilizing flow cytometry. First, 3×10^5 MCF-7 cells were seeded into each well, treated with 200 μg/mL of each nanoparticle, and were incubated for 24 h. After that, the trypsinized cells were washed by PBS and were suspended in *Annexin-V* binding buffer. Finally, 5 and 10 μL of *FITC-Annexin-V/PI* solution were added into the driven solution, and the flow cytometer counted cells.

2.5. Caspase-3, −8, and − 9 multiplex activity assay

Caspase activity kit was used to quantify caspase-3, −8, and − 9 activity in apoptotic cells lysed through incubation with nanomaterials (44 μg/mL) for 24 h in a 5 % CO_2 atmosphere. The lysate was then centrifuged at 600 *g* for 5 min, and followingly 50 μL of supernatant was added to a new test tube. Subsequently, 10 mM DTT dissolved in 50 μL of 2× reaction buffer was added to each sample. Then ρNA-conjugated substrate (200 μM) was added to each tube and followed by incubation at 37 °C for 2 h. Eventually, the samples were read at 400 nm for absorbencies to determine caspase activity.

2.6. Antibacterial assessment of the nanomaterials

The dilution method determined minimum inhibitory concentration (MIC) and minimum bacterial concentration (MBC), i.e., decreasing the concentrations of AgMOF and GO-AgMOF starting from 500 μg/mL. A 0.5 McFarland suspension of *S. mutans* and *S. aureus* was made in physiological serum with 0.1 optical density. Subsequently, each sample's bacteria-containing solution was added to reach the bacteria concentration of 10^5 per mL. Next, the two groups of bacteria samples and the control sample were incubated at 37 °C for 24 h. The samples' lowest concentration that does not show any bacteria growth would be recorded as MIC. The samples were also cultured in agar plates, and the concentration for which no bacteria growth is observed would be recorded as MBC.

Following the standards established by the Clinical and Laboratory Standards Institute (CLSI), M-H Broth is used for determining MIC. To achieve this, the extracted methanol was diluted to a concentration range of 7.8–500 mg/mL and then added to the test tubes containing the medium in a row. After incubating the tubes at 37 °C for 24 h, the bacteria growth was investigated to determine the minimum concentration which prevented bacterial growth, regarded as MIC. Furthermore, 10 μL of each well's media was moved to a Mueller Hinton agar (MHA) plate and thus incubated for another 24 h while in contact with oxygen. Consequently, the lowest concentration with no bacterial growth is considered as MBC. Each test was repeated 3 times to ensure precision.

The overlay method was used to determine the inhibition zone diameter. First, 5 mL of Luria-Bertani (LB) culture medium was added to a sterile plate to form the first layer; then, the second layer was formed by adding another 15 mL. Moreover, 50 μL of different nanomaterials' concentrations were used to form 6-mm-diameter disks. Hence, the plates were incubated at 37 °C for 24 h. After that, the zones' diameters were measured, and the samples were photographed by a digital camera.

2.7. Apoptotic gene expressions analysis by qPCR

A qPCR test has been performed to quantify BAX and BCL2 genes level after treating SW480 cells with AgMOF and GO-AgMOF. For this purpose, SW480 cells (5×10^5 cells per well) were seeded in a plate in contact with the nanomaterials and incubated for 24 h. An RNA-isolation kit was used to isolate mRNA. Then reverse transcription converts mRNA to its complementary DNA (cDNA) using PrimeScript, cDNA Synthesis Kit. Finally, the gene expression was studied by ABI 7300 qPCR system using the 2(-Delta Delta C(T)) method (DDCT method).

2.8. DNA fragmentation test

The DNA fragmentation was detected by staining the treated cells with a Hoechst fluorescence stain. SW480 cells were grown on sterile, non-adherent, 12-well plates overnight and treated with nanomaterials at IC50 concentration. Then 200 μL of paraformaldehyde was added to the fixed cells and incubated for 20 min at room temperature. After that, the samples were washed by PBS, and followingly were stained with 100 ng/mL of Hoechst stain and left for 10 h. Finally, the samples were investigated by optical microscopy.

2.9. Ion release stability of the nanocomposites

The leaching experiments of the nanocomposites were preliminarily investigated by determining the amount of silver ions released from the AgMOF and GO-AgMOF. Each material (100 mg) sample was stored in 50 mL of DI water with continuous shaking (150 rpm) for 15 days. The samples were centrifuged first for each experiment to collect the powders, and aliquots were taken for inductively coupled plasma mass spectrometry (ICP-MS). The concentration of silver ions in the DI water solution was determined by ICP-MS (AA300 Agilent Technologies).

3. Results & discussion

Dysregulation of apoptotic pathways occurs commonly in several types of malignancies [47]. Using external stimulants like nanomaterials to induce apoptosis is highly efficient in treating cancer [48]. Previous studies showed nanomaterials are more biocompatible than conventional therapeutics such as chemotherapy surgery and radiotherapy [49]. In addition, specificity and fewer side effects give nanomaterials an advantage in treating cancer [50,51]. Here, after measuring the size of particles using transmission electron microscopy (TEM) (Fig. 1c-d), we approached several methods to investigate apoptosis and predict its mechanism as a result of nanomaterials treatment.

3.1. Unique morphology of AgMOF results in its tumor specificity

TEM was employed to study the morphology of AgMOF and GO-AgMOF nanomaterials (Fig. 1c-d). The bulk crystalline structure of AgMOF nanomaterials is observed in TEM images (Fig. 1c). TEM images are used to determine the particle size, one of the most important parameters when using nanomaterials. AgMOFs are around 20 nm in diameter. Compared to the normal vessels with a pore size of 6 to 12 nm, tumor vessels are more permeable with much larger pores (from 100 to 780 nm). Therefore, nanomaterials can specifically penetrate the tumors but not the normal vessels [52]. It can be concluded that AgMOF nanomaterials have desired size (Fig. 1c). Furthermore, the TEM image of GO-AgMOF nanocomposite (Fig. 1.d) shows that AgMOF are embedded adequately into GO layers same as what has been reported by Firouzjaei et al. [46]. Along with TEM images, FTIR spectra of the GO, AgMOF, and GO-AgMOF nanoparticles are shown in Fig. 1e. Regarding the GO spectrum, the broad peak at ~3411 cm^{-1} is attributed to –OH stretching [53]. Carbonyl-associated peaks are observed at 1716 cm^{-1} and 1619 cm^{-1}, respectively assigned to C═O bonds and hydroxyl group of carbonyl [54]. In addition, hydroxyl group of tertiary is responsible for the peak at 1169 cm^{-1} [55]. Similar spectra are observed for AgMOF and GO-AgMOF. However, the broader peak of GO-AgMOF compared to that of Ag-MOF in the range of 2600–3600 cm^{-1} is due to the presence of GO in the structure of GO-AgMOF [55]. The peaks at 700–900 cm^{-1} are representative of C—H bonding, and the peaks at 1164 and 1195 cm^{-1} are corresponded to C—O group [56,57]. The peaks detected in the range of 1390–1450 cm^{-1} are associated to C═C stretching [58,59]. The three peaks appeared approximately at 1682, 1666, and 1607 cm^{-1} unveils the reaction between silver ions and carbonyl groups in trimesic acid [60].

Fig. 1f-k presents the XPS spectra of GO, AgMOF, and GO-AgMOF nanomaterials. Obviously, the peaks associated to C 1 s and O 1 s are observed in all three spectra. The peaks assigned to Ag 3d are appeared in the XPS spectra of AgMOF and GO-AgMOF due to the presence of silver in the structures. Deconvolution of the XPS peaks led to four sub-peaks for carbon resulting from different functional groups in GO (Fig. 1g). The peak centered at ~284 eV is attributed to the bonds from non-oxygenated carbons including C—C and C═C [61]. Two peaks at ~286 and ~ 287 eV are assigned to C–OH and C–O–C, respectively [62]. Additionally, the peak at ~288 eV supports the presence of carboxylate carbon [63]. Resulted from XPS measurements, the C/O ratio in GO is about 2.5, and in agreement with the reported values in the literature [64]. The C 1 s decomposed peak in the spectra of AgMOF and GO-AgMOF indicates three peaks (Fig. 1h and i); these peaks are at ~284.7, ~285.2, and ~ 288.7 eV, which are respectively assigned to carbon-carbon bonds (C—C and C═C), C—O, and C═O. Moreover, the extra peak at ~286.9 eV in the spectrum of GO-AgMOF is caused by the epoxy groups of GO in the structure, verifying the presence of GO. Furthermore, Ag $3d_{3/2}$ and $3d_{5/2}$ and peaks are observed at ~374.3 and ~ 368.2 eV resulting from bondage between silver and oxygen atoms (Fig. 1j and k) [65]. Fig. 1l shows the sharp XRD peak at about $2\theta = 9.7^\circ$ represents the (002) crystalline plane of GO with a d-spacing of 0.91 nm [66], and the peaks at about 2θ = 39.1°, 43.9°, 65.4° and 75.0° are respectively assigned to (111), (200), (220), and (311) face centered cubic planes of silver [67].

Average sizes of the three nanoparticles are calculated via DLS analysis and the results are depicted on Fig. 2a. The proper dispersion with no agglomeration of the AgMOF nanoparticles in GO are congruent with the average size of GO-AgMOF. The small difference between the GO-AgMOF size and the sum of AgMOF and GO sizes reveals the trivial level of agglomeration. XRD was employed to confirm the formation of crystalline structures resulted from presence of AgMOF nanoparticles on GO (Fig. 1l). UV–vis spectroscopy was performed separately for the GO, AgMOF, and GO-AgMOF to determine the level of AgMOF interaction with GO; the result is presented in Fig. 2b. The sharp peak at ~213 nm in the absorption spectrum of GO is caused by the electronic π-π* transition of aromatic C—C bonds and the shoulder peak appeared around 300 nm is due to the n-π* transition of C═O bonds [68,69]. The observed peak at around 206 nm for AgMOF is shifted to 209 nm in the spectrum of GO-AgMOF nanocomposite, revealing the interaction between the GO and GO-AgMOF nanoparticles.

3.2. Nanomaterials showed cytotoxicity to cancer cells

The cell viability was measured after nanomaterials treatment by the MTT assay. The results indicate that both AgMOF and GO-AgMOF show cytotoxicity against the SW480 cancer cell line in a dose-dependent

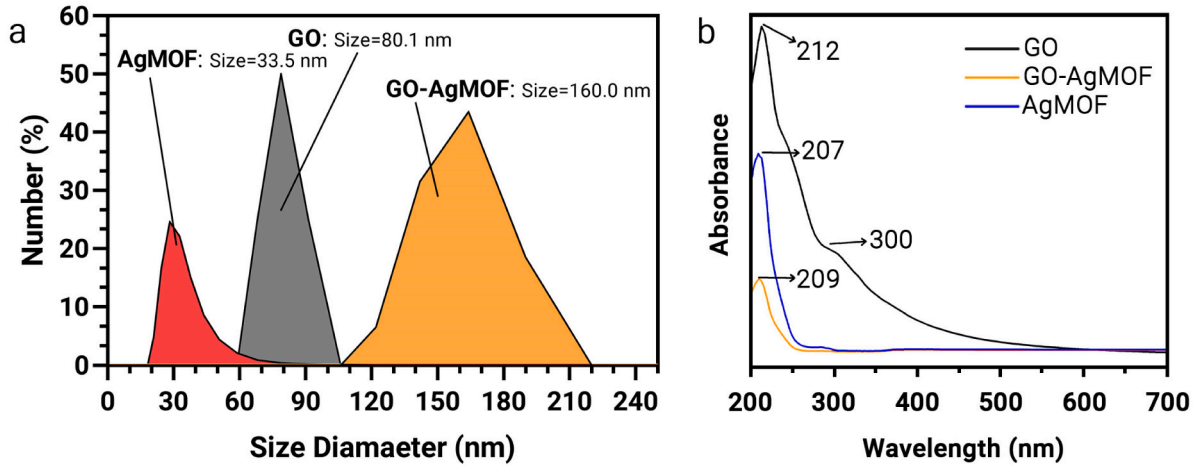

Fig. 2. (a) Size distribution of GO, AgMOF, and GO-AgMOF. The average size of the nanomaterials is reported inside the graph. (b) UV–vis absorption spectra of GO, AgMOF, and GO-AgMOF.

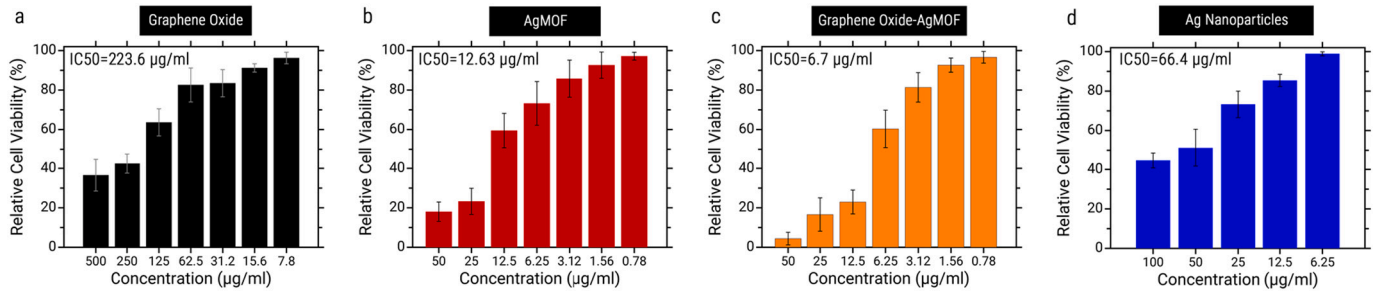

Fig. 3. Relative viability of SW480 cells versus (a) GO, (b) AgMOF, (c) GO-AgMOF, and (d) Ag nanoparticles concentration in comparison to the control group.

manner. Fig. 3 presents the relative cell viability versus nanomaterials concentration. As expected, the cell viability was decreased by increasing nanomaterials concentration. Drugs can be compared to one another using the IC50 values which indicate drug concentration that inhibits growth of tumor cell colony by half. Low IC50 value means that the drug is effective at low concentrations, and thus will show lower systemic toxicity when administered to the patient [70]. As shown in Fig. 3, the IC50 values for GO, Ag nanoparticles, AgMOF, and GO-AgMOF are 223.6, 66.4, 12.63, and 6.7 µg/mL respectively. So, it can be concluded that GO-AgMOF has the least IC50 and is more efficient in treating cancer. One possible reason for more toxicity of AgMOF in comparison to Ag is intracellular silver delivery of AgMOF controlled by the extracellular pH, which has been described by ploetz et al. [71]. An essential step in MOF toxicity is its decomposition to Ag ions and BTC in lysosome and delivering high amounts of silver ions into the cell. Nanoscale MOFs with great surface area play a positive role in the adhesion of cells to the GO-AgMOF react with cancerous cells and release Ag ions which is toxic while the aggregation of pure Ag nanoparticles leads to reduction of active specific surface area of Ag nanoparticles and its toxicity in contact to cancerous cells [72]. Another possible mechanism may be that decreased pH value due to BTC presence caused cell death. The addition of GO to AgMOF has a synergic effect and decreases tumor cell viability. AgMOFs' toxicity is due to their ionic form and nano-metric structure. Determining the exact portion of each mechanism is challenging. On the one hand, silver ions toxicity is attributed to nanomaterials transformation in biological media, ion release, and interlinkage with biological macromolecules [73]. On the other hand, nanomaterials' high surface area and surface reactivity assist toxicity [74]. AgMOF interacts with the proteins on the cell membrane and stops cell proliferation. They also penetrate mitochondria selectively, causing dysfunction, reactive oxygen species (ROS) generation, and damaging nucleic acid and proteins inside the cell [73–76]. Similarly, GO nanosheets decrease cell viability, cause apoptosis, ruin membrane integrity, change cell morphology, damage DNA, and prohibit cell adhesion by accelerating ROS generation and activating the mitochondrial apoptosis pathway [77]. Conclusively, the cytotoxicity of AgMOF and GO-AgMOF has a significant role in the anti-tumor activity and reduces tumor progression [77].

3.3. AgMOF and GO-AgMOF induce apoptosis by increasing caspase activity

Flow cytometry was used to calculate the percentage of apoptotic cells, and also track apoptotic changes by concurrent staining with Annexin-V-APC conjugate and propidium iodide (PI) (Fig. 4). Based on our results, both AgMOF and Go-AgMOF nanomaterials can induce apoptosis in SW480 cells. As depicted in Fig. 4, untreated cells did not show any remarkable apoptosis. AgMOF treated cells had 16.1 and 65.4 % early and late apoptotic cells, respectively. The percent of early and late apoptotic cells for GO-AgMOF were 12.9 and 84.3 %, respectively. It is rational that the cytotoxic effect of GO-AgMOF nanomaterials acts slower in comparison to AgMOF nanomaterials. Because AgMOF particles, due to their smaller sizes (supported by TEM images), can easily pass through the cell membrane by diffusion while larger GO-AgMOF particles penetrate the cell with a more time-consuming process. Hence, it takes a longer time for GO-AgMOF to cause cell death.

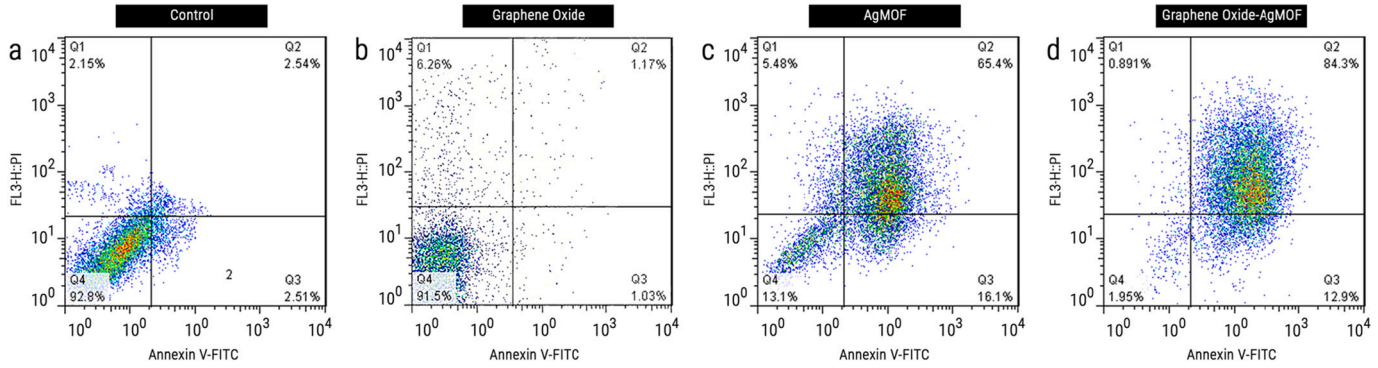

Fig. 4. Flow cytometry images of (a) control, (b) GO, (c) AgMOF, and (d) GO-AgMOF samples.

However, after GO-AgMOF penetration, sharp edges of GO nanosheets damage the cell membrane leading to loss of membrane integrity. PI enters the cell through the lost membrane and flags late apoptosis [78]. So, the synergic effect of AgMOF and GO toxicity causes more percentage of late apoptosis in comparison to AgMOF [79]. In general, it is clear that the number of the cells in the early and late stages of apoptosis increased after treating with both AgMOF and GO-AgMOF nanomaterials which confirms that these nanomaterials can induce apoptosis.

Caspase activity plays a fundamental role in the execution phase of cell apoptosis [80]. Induction of caspase-8 and -9 (initiator caspase) and caspase-3 (effector caspase) expression after treating SW480 cells with AgMOF and GO-AgMOF nanomaterials was measured as markers of apoptosis. It has been known that caspase-8 cleaves and activates caspase-3 (effector caspase), which triggers the extrinsic pathway. Caspase-3 activation is the irreversible point in the apoptosis process [81]. Caspase-3 activation happens by cleavage and translocation of the activated caspase into the nucleus, followed by DNA fragmentation, which is essential in the first steps of apoptosis. The DNA fragmentation induced by caspase activation can be detected by Hoechst staining. Simultaneously, the intrinsic or mitochondrial route needs activation of caspase-9 to initiate caspase-3 activation for apoptotic cell death [81–84].

As shown in Fig. 5, the caspase activity in cells treated with AgMOF and GO-AgMOF nanomaterials increased significantly compared to the

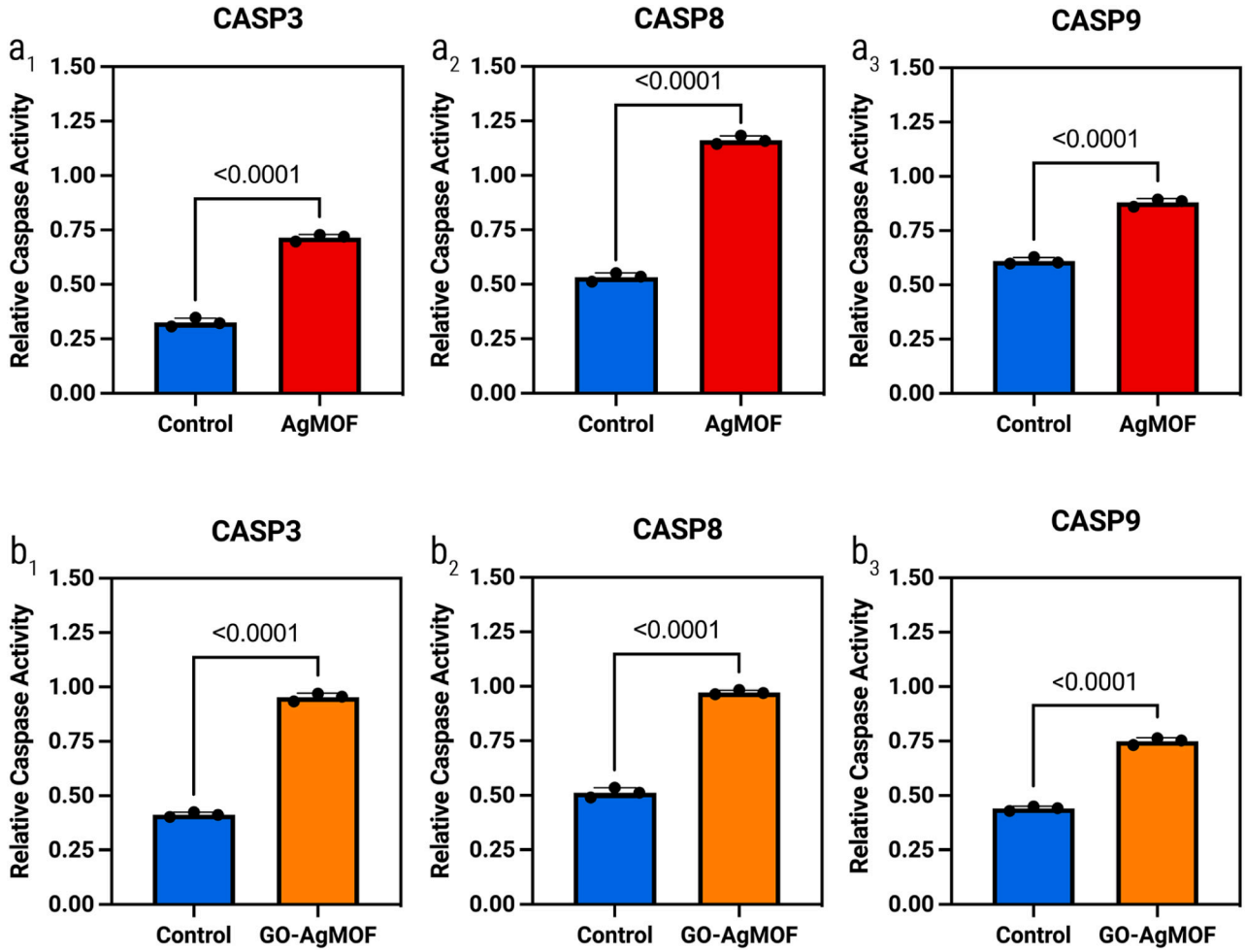

Fig. 5. Caspase-3, −8 and − 9 activity of SW480 cells in contact with (a) AgMOF and (b) GO-AgMOF nanomaterials.

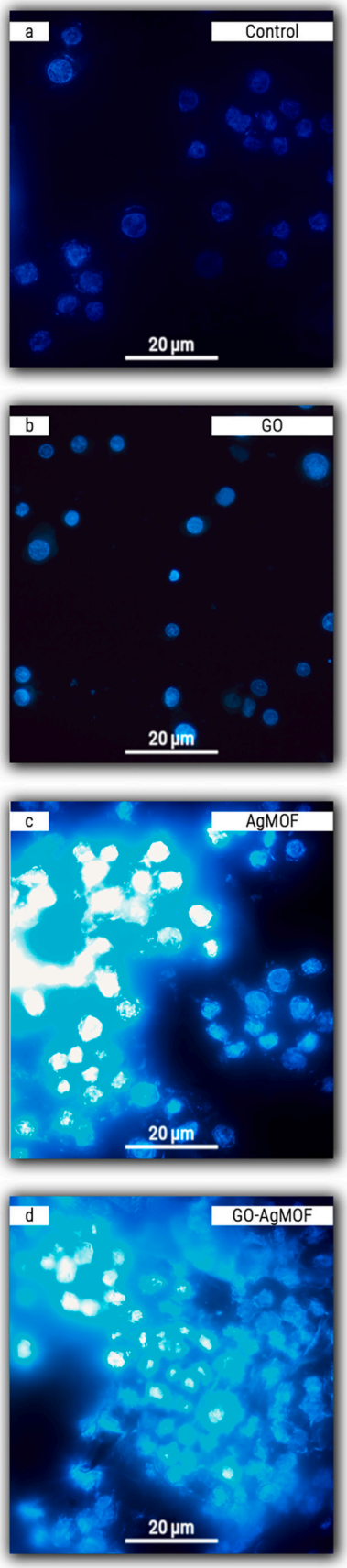

Fig. 6. Hoechst staining of SW480 cells in (a) control, (b) GO, (c) AgMOF, and (d) GO-AgMOF nanomaterials groups.

control group. The higher caspase expression level in treated groups reveals apoptosis, leading to abnormal cell elimination, eventually reducing tumor progression. Significant increase in caspase-3, −8, and − 9 activity in treated cells with AgMOF and 2.3-, 1.89-, and 1.70-fold increase in treated cells with GO-AgMOF indicates the nanomaterials' effectiveness in increasing apoptosis.

As stated above, caspase activation leads to DNA fragmentation which is one of the early stages of apoptosis [83]. The DNA fragmentation of cancerous cells due to the addition of nanomaterials was analyzed using Hoechst fluorescent stain (Fig. 6). After treating SW480 cells with 20 µg/mL of nanomaterials, cells started to show apoptotic characteristics such as DNA fragmentation. As shown in Fig. 6, the cells have regular, rounded morphology and intact nuclear structure in the control group. In treated samples, caspase cascade activation cleaves the determined substrate, which is responsible for DNA repair. Fragmented nuclei, as another hallmark of apoptosis [85], are shown as granules with various sizes stained homogeneously. DNA is shown in a dispersed form. Previous studies show that GO changes the membrane of cancerous cells by targeting the microtubules of the cytoskeleton and damaging them [86]. So, the cell loses its original shape and structural integrity [86].

3.4. Apoptotic gene expressions analysis by qPCR

Pro-apoptotic BAX and anti-apoptotic BCl2 genes are members of BCl2 family proteins that play essential roles as regulators in the mitochondrial apoptotic pathways [87,88]. BCl2 suppresses apoptosis while BAX contains BH1–3 domains and creates proteolipid pores responsible for cytochrome C release that permeabilizes the outer membrane of mitochondria [89–92]. Therefore, increasing BAX/BCl2 expression ratio causes caspase-3 activation and indicates apoptosis which helps in the cancer treatment [93]. Here, we carried out a qPCR test to analyze the changes in expression of these genes after nanomaterials addition (Fig. 7). BAX/BCL2 ratio significantly increased for both AgMOF and GO-AgMOF nanomaterials, showing caspase-dependent apoptosis is the mechanism leading to cell death.

3.5. The stability of nanocomposites

A promising feature of MOFs is their potential to prevent the uncontrolled release of ions during their long-term operation. As shown in Fig. 8, both AgMOF and GO-AgMOF released <50 (µg/L) silver ions. MOF structure acts as reservoirs of silver, promoting the sustained and gradual leaching of this metal ion to achieve prolonged anticancer activity of the nanocomposites. However, AgMOF has a marginal higher release rate compared to GO-AgMOF. However, the chemical structure of GO-AgMOF provides an insight into this feature. The possible interaction between silver ions and negatively charged functional groups GO me be responsible for lower release rates of GO-AgMOF compared to AgMOF.

4. Conclusion

Our findings indicate that AgMOF and GO-AgMOF nanomaterials cause cancerous cells apoptosis and have antibacterial properties. These nanomaterials induce apoptosis via intrinsic and extrinsic pathways by activating caspase-3, −8, and − 9 in a dose-dependent manner. MTT test results show a reduction in SW480 cells viability with increasing concentrations. Increasing BAX/BCl2 ratio and percentage of early and late apoptotic cells compared to necrotic cells and fragmented nucleus and DNA are all evidence that confirms apoptosis. Furthermore, the results obtained from measuring MBC/MIC showed the great antibacterial activity of AgMOF and GO-AgMOF against *S. mutans* and *S. aureus* and the higher toxicity of GO-AgMOF compared to AgMOF. The MBC/MIC ratio is ≤4 for all four cases, verifying that both nanomaterials can be considered bactericides. The antibacterial activities are similar to

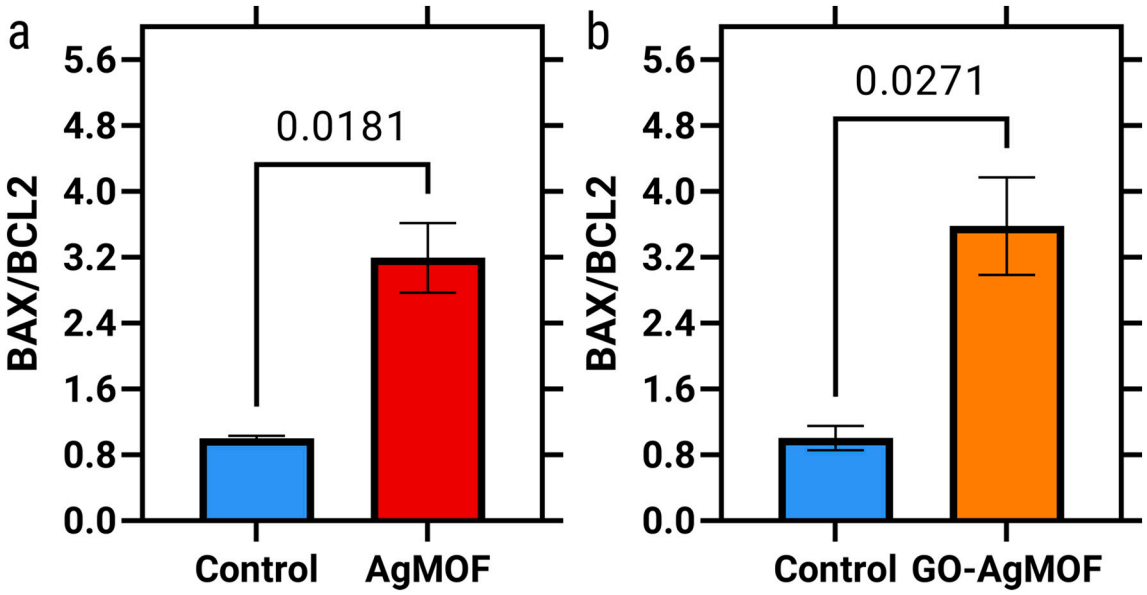

Fig. 7. The BAX/BCL2 mRNA expression ratio of (a) AgMOF and (b) GO-AgMOF.

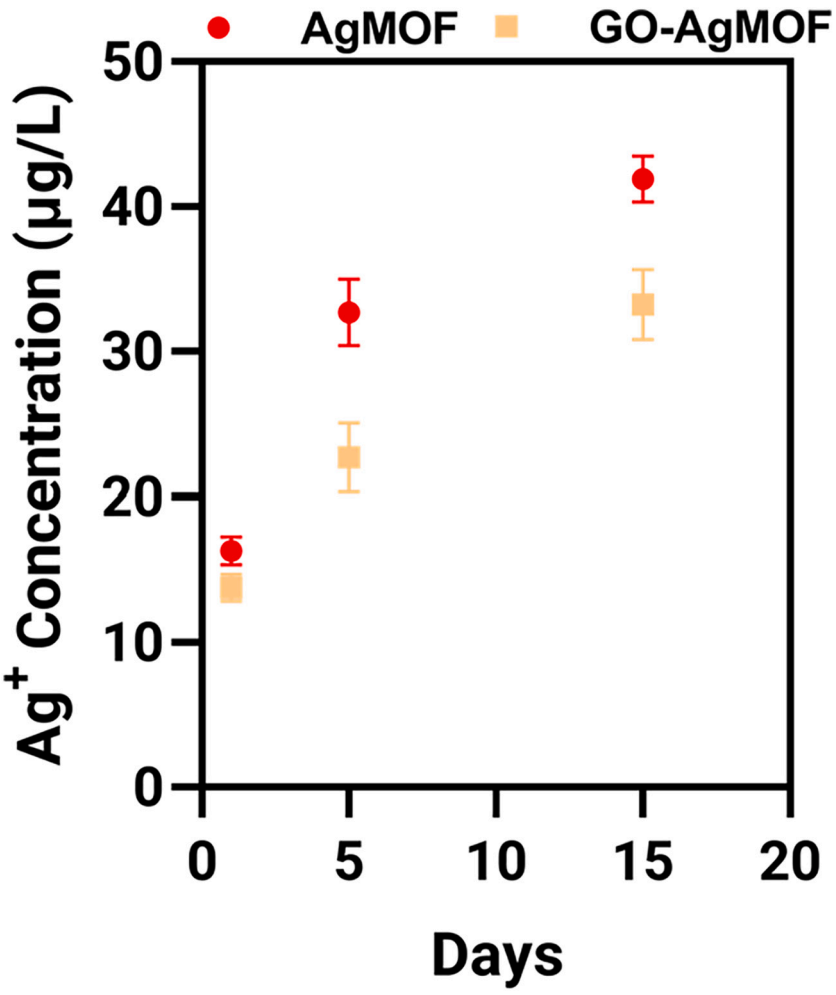

Fig. 8. The release rate of Silver ions was measured by ICP-MS for 15 days.

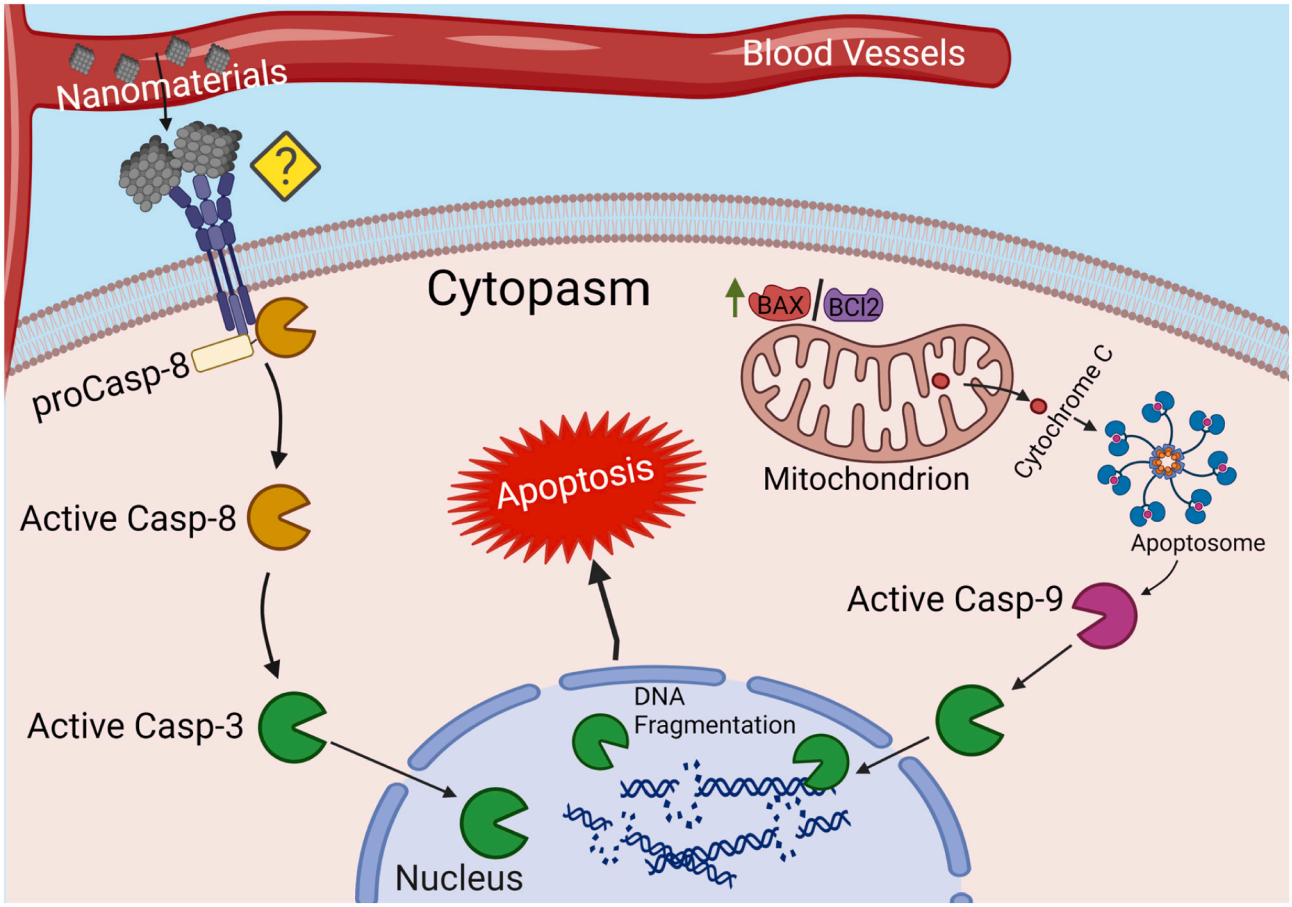

Fig. 9. The graphical abstract of the antineoplastic effect of nanomaterials.

commercially available anticancer drugs such as thioguanine and methotrexate against *S. aureus*. This preliminary cell cytotoxicity study of AgMOF and GO-AgMOF nanomaterials could provide a pathway to understanding cell-nanomaterials interaction's holistic mechanism. Finally, our results suggest that both AgMOF and GO-AgMOF nanomaterials could be potential antimicrobial candidates for anticancer therapy using the apoptosis method. Fig. 9 schematically summarizes the mechanism behind the antineoplastic effect of AgMOF and GO-AgMOF.

CRediT authorship contribution statement

Yashar Rezaeipour: Data curation, Formal analysis, Investigation, Visualization, Writing – original draft. **Ehsan Zolghadr:** Data curation, Formal analysis, Investigation, Visualization, Writing – original draft. **Parvin Alizadeh:** Funding acquisition, Project administration, Resources, Supervision. **Ghazal Sadri:** Data curation, Formal analysis, Investigation, Visualization, Writing – original draft. **Evan K. Wujcik:** Validation, Resources, Writing – review & editing. **Farhad Akbari Afkhami:** Data curation, Validation, Writing – review & editing. **Mark Elliott:** Conceptualization, Funding acquisition, Project administration, Resources, Supervision, Visualization, Writing – review & editing. **Mostafa Dadashi Firouzjaei:** Data curation, Formal analysis, Investigation, Visualization, Conceptualization, Project administration, Supervision, Writing – review & editing.

Declaration of competing interest

The authors declare that they have no known competing financial interests or personal relationships that could have appeared to influence the work reported in this paper.

Appendix A. Supplementary data

Supplementary data to this article can be found online at https://doi.org/10.1016/j.bioadv.2022.213013.

References

[1] J. Rao, Y. Yang, H. Pan Bei, C.Y. Tang, X. Zhao, Antibacterial nanosystems for cancer therapy, Biomater. Sci. 8 (2020) 6814–6824, https://doi.org/10.1039/d0bm01537g.
[2] D. Ficai, A. Ficai, E. Andronescu, Advances in cancer treatment: role of nanoparticles, Nanomater. - Toxic. Risk Assess. (2015) 1–22, https://doi.org/10.5772/60665.
[3] M.A. Feitelson, A. Arzumanyan, R.J. Kulathinal, S.W. Blain, R.F. Holcombe, J. Mahajna, M. Marino, M.L. Martinez-Chantar, R. Nawroth, I. Sanchez-Garcia, D. Sharma, N.K. Saxena, N. Singh, Vlachostergios Panagiotis, S. Guo, K. Honoki, H. Fujii, A.G. Georgakilas, A. Amedei, E. Niccolai, A. Amin, S.S. Ashraf, C. S. Boosani, G. Guha, M.R. Ciriolo, K. Aquilano, S. Chen, S.I. Mohammed, A.S. Azmi, D. Bhakta, D. Halicka, S. Nowsheen, Sustained proliferation in cancer: therapeutic targets, Semin. Cancer Biol. 35 (2016) 25–54, https://doi.org/10.1016/j.semcancer.2015.02.006.Sustained.
[4] J. Klastersky, D. Daneau, A. Verhest, Causes of death in patients with cancer, Eur. J. Cancer 8 (1972) 149–154, https://doi.org/10.1016/0014-2964(72)90036-9.
[5] Z.H. Siddik, Mechanisms of action of cancer chemotherapeutic agents: DNA-interactive alkylating agents and antitumour platinum-based drugs, Cancer Handb. (2005), https://doi.org/10.1002/0470025077.chap84b.
[6] W.B. Parker, Enzymology of purine and pyrimidine antimetabolites used in the treatment of cancer, Chem. Rev. 109 (2009) 2880–2893, https://doi.org/10.1021/cr900028p.
[7] R. Thirumaran, G.C. Prendergast, P.B. Gilman, Cytotoxic Chemotherapy in Clinical Treatment of Cancer, Elsevier Inc, 2007, https://doi.org/10.1016/B978-012372551-6/50071-7.
[8] E. Dickens, S. Ahmed, Principles of cancer treatment by chemotherapy, Surg. (United Kingdom) 36 (2018) 134–138, https://doi.org/10.1016/j.mpsur.2017.12.002.

[9] G. Mohan, A.H. T P, J. A J, S.D. K M, A. Narayanasamy, B. Vellingiri, Recent advances in radiotherapy and its associated side effects in cancer—a review, J. Basic Appl. Zool. (2019) 80, https://doi.org/10.1186/s41936-019-0083-5.
[10] L.Y. Ramirez, S.E. Huestis, T.Y. Yap, S. Zyzanski, D. Drotar, E. Kodish, Potential chemotherapy side effects: what do oncologists tell parents? Pediatr. Blood Cancer 52 (2009) 497–502, https://doi.org/10.1002/pbc.21835.
[11] K. Nurgali, R.T. Jagoe, R. Abalo, Editorial: adverse effects of cancer chemotherapy: anything new to improve tolerance and reduce sequelae? Front. Pharmacol. 9 (2018) 1–3, https://doi.org/10.3389/fphar.2018.00245.
[12] P.V. Rao, D. Nallappan, K. Madhavi, S. Rahman, L. Jun Wei, S.H. Gan, Phytochemicals and biogenic metallic nanoparticles as anticancer agents, Oxidative Med. Cell. Longev. 2016 (2016), https://doi.org/10.1155/2016/3685671.
[13] K. Sztandera, M. Gorzkiewicz, B. Klajnert-Maculewicz, Gold nanoparticles in cancer treatment, Mol. Pharm. 16 (2019) 1–23, https://doi.org/10.1021/acs.molpharmaceut.8b00810.
[14] M. Jeyaraj, G. Sathishkumar, G. Sivanandhan, D. MubarakAli, M. Rajesh, R. Arun, G. Kapildev, M. Manickavasagam, N. Thajuddin, K. Premkumar, A. Ganapathi, Biogenic silver nanoparticles for cancer treatment: an experimental report, Colloids Surf. B: Biointerfaces 106 (2013) 86–92, https://doi.org/10.1016/j.colsurfb.2013.01.027.
[15] Y. Gao, K. Chen, J.L. Ma, F. Gao, Cerium oxide nanoparticles in cancer, Onco. Targets. Ther. 7 (2014) 835–840, https://doi.org/10.2147/ott.s62057.
[16] D. Acharya, S. Satapathy, P. Somu, U.K. Parida, G. Mishra, Apoptotic effect and anticancer activity of biosynthesized silver nanoparticles from marine algae Chaetomorpha linum extract against human colon cancer cell HCT-116, Biol. Trace Elem. Res. (2020), https://doi.org/10.1007/s12011-020-02304-7.
[17] A. Aghebati-Maleki, S. Dolati, M. Ahmadi, A. Baghbanzhadeh, M. Asadi, A. Fotouhi, M. Yousefi, L. Aghebati-Maleki, Nanoparticles and cancer therapy: perspectives for application of nanoparticles in the treatment of cancers, J. Cell. Physiol. 235 (2020) 1962–1972, https://doi.org/10.1002/jcp.29126.
[18] J.K. Patra, G. Das, L.F. Fraceto, E.V.R. Campos, M.D.P. Rodriguez-Torres, L. S. Acosta-Torres, L.A. Diaz-Torres, R. Grillo, M.K. Swamy, S. Sharma, S. Habtemariam, H.S. Shin, Nano based drug delivery systems: recent developments and future prospects 10 Technology 1007 Nanotechnology 03 Chemical Sciences 0306 Physical Chemistry (incl. Structural) 03 Chemical Sciences 0303 Macromolecular and Materials Chemistry 11 Medical and He, J. Nanobiotechnol. 16 (2018) 1–33, https://doi.org/10.1186/s12951-018-0392-8.
[19] S.A.A. Rizvi, A.M. Saleh, Applications of nanoparticle systems in drug delivery technology, Saudi Pharm. J. 26 (2018) 64–70, https://doi.org/10.1016/j.jsps.2017.10.012.
[20] Q. Mu, B. Yan, Editorial: nanoparticles in cancer therapy-novel concepts, mechanisms, and applications, Front. Pharmacol. 9 (2019) 2018–2020, https://doi.org/10.3389/fphar.2018.01552.
[21] M. Hosseini, M. Haji-Fatahaliha, F. Jadidi-Niaragh, J. Majidi, M. Yousefi, The use of nanoparticles as a promising therapeutic approach in cancer immunotherapy, Artif. Cells, Nanomedicine, Biotechnol. 44 (2016) 1051–1061.
[22] W. Park, Y.-J. Heo, D.K. Han, New opportunities for nanoparticles in cancer immunotherapy, Biomater. Res. 22 (2018) 1–10.
[23] J. Jia, Y. Zhang, Y. Xin, C. Jiang, B. Yan, S. Zhai, Interactions between nanoparticles and dendritic cells: from the perspective of cancer immunotherapy, Front. Oncol. 8 (2018), https://doi.org/10.3389/fonc.2018.00404.
[24] G.M. Abdel-Fattah, E.E. Hafez, M.E. Zaki, N.M. Darwesh, Cloning and expression of alpha hemolysin toxin gene of Staphylococcus aureus against human cancer tissue, Int. J. Appl. Sci. Biotechnol. 5 (2017) 22–29.
[25] F. Bray, J. Ferlay, I. Soerjomataram, R.L. Siegel, L.A. Torre, A. Jemal, Global cancer statistics 2018: GLOBOCAN estimates of incidence and mortality worldwide for 36 cancers in 185 countries, CA. Cancer J. Clin. 68 (2018) 394–424.
[26] M. Karin, T. Lawrence, V. Nizet, Innate immunity gone awry: linking microbial infections to chronic inflammation and cancer, Cell 124 (2006) 823–835.
[27] B.L. Ferguson, S. Barber, I.H. Asher, C.R. Wood, Role of Oral microbial infections in Oral cancer, Dent. Clin. N. Am. 61 (2017) 425–434.
[28] K. Zheng, M.I. Setyawati, D.T. Leong, J. Xie, Antimicrobial gold nanoclusters, ACS Nano 11 (2017) 6904–6910.
[29] S. Zhu, X. Wang, S. Li, L. Liu, L. Li, Near-infrared-light-assisted in situ reduction of antimicrobial peptide-protected gold nanoclusters for stepwise killing of bacteria and cancer cells, ACS Appl. Mater. Interfaces 12 (2020) 11063–11071.
[30] M.D. Firouzjaei, A.A. Shamsabadi, S.A. Aktij, S.F. Seyedpour, M. Sharifian Gh, A. Rahimpour, M.R. Esfahani, M. Ulbricht, M. Soroush, Exploiting synergetic effects of graphene oxide and a silver-based metal–organic framework to enhance antifouling and anti-biofouling properties of thin-film nanocomposite membranes, ACS Appl. Mater. Interfaces 10 (2018) 42967–42978.
[31] Y. Wu, J. Han, P. Xue, R. Xu, Y. Kang, Nano metal-organic framework (NMOF)-based strategies for multiplexed microRNA detection in solution and living cancer cells, Nanoscale 7 (2015) 1753–1759, https://doi.org/10.1039/c4nr05447d.
[32] M. Giménez-Marqués, T. Hidalgo, C. Serre, P. Horcajada, Nanostructured metal-organic frameworks and their bio-related applications, Coord. Chem. Rev. 307 (2016) 342–360, https://doi.org/10.1016/j.ccr.2015.08.008.
[33] S.F. Seyedpour, A.Arabi Shamsabadi, S.Khoshhal Salestan, M.Dadashi Firouzjaei, M.Sharifian Gh, A. Rahimpour, F.Akbari Afkhami, M.A. Elliott, A. Tiraferri, M.Reza Shirzad Kebria, Tailoring the biocidal activity of novel silver-based metal azolate frameworks, ACS Sustain. Chem. Eng. 8 (2020) 7588–7599.
[34] S. Galdiero, A. Falanga, M. Cantisani, A. Ingle, M. Galdiero, M. Rai, in: Silver Nanoparticles as Novel Antibacterial and Antiviral Agents, 2014, pp. 565–594, https://doi.org/10.1142/9789814520652_0015.
[35] P. Vaid, P. Raizada, A.K. Saini, R.V. Saini, Biogenic silver, gold and copper nanoparticles - a sustainable green chemistry approach for cancer therapy, Sustain. Chem. Pharm. 16 (2020), 100247, https://doi.org/10.1016/j.scp.2020.100247.
[36] M.X. Wu, Y.W. Yang, Metal-organic framework (MOF)-based drug/cargo delivery and cancer therapy, Adv. Mater. 29 (2017) 1–20, https://doi.org/10.1002/adma.201606134.
[37] R. Tong, J. Cheng, Paclitaxel-initiated, controlled polymerization of lactide for the formulation of polymeric nanoparticulate delivery vehicles, Angew. Chemie Int. Ed. 47 (2008) 4830–4834.
[38] P. Yang, S. Gai, J. Lin, Functionalized mesoporous silica materials for controlled drug delivery, Chem. Soc. Rev. 41 (2012) 3679–3698.
[39] J. Park, Q. Jiang, D. Feng, L. Mao, H.-C. Zhou, Size-controlled synthesis of porphyrinic metal–organic framework and functionalization for targeted photodynamic therapy, J. Am. Chem. Soc. 138 (2016) 3518–3525.
[40] V.V. Neklyudov, N.R. Khafizov, I.A. Sedov, A.M. Dimiev, New insights into the solubility of graphene oxide in water and alcohols, Phys. Chem. Chem. Phys. 19 (2017) 17000–17008, https://doi.org/10.1039/c7cp02303k.
[41] V. Jabbari, J.M. Veleta, M. Zarei-Chaleshtori, J. Gardea-Torresdey, D. Villagrán, Green synthesis of magnetic MOF@GO and MOF@CNT hybrid nanocomposites with high adsorption capacity towards organic pollutants, Chem. Eng. J. 304 (2016) 774–783, https://doi.org/10.1016/j.cej.2016.06.034.
[42] Y. Zheng, S. Zheng, H. Xue, H. Pang, Metal-organic frameworks/graphene-based materials: preparations and applications, Adv. Funct. Mater. 28 (2018) 1–28, https://doi.org/10.1002/adfm.201804950.
[43] J. Wang, P. Wang, Y. He, X. Liu, S. Wang, C. Ma, X. Tian, J. Wang, X. Wu, Graphene oxide inhibits cell migration and invasion by destroying actin cytoskeleton in cervical cancer cells, Aging (Albany. NY) 12 (2020) 17625–17633, https://doi.org/10.18632/AGING.103821.
[44] Y. Yang, A.M. Asiri, Z. Tang, D. Du, Y. Lin, Graphene based materials for biomedical applications, Mater. Today 16 (2013) 365–373, https://doi.org/10.1016/j.mattod.2013.09.004.
[45] S. Wang, B. Ye, C. An, J. Wang, Q. Li, H. Guo, J. Zhang, Exploring the coordination effect of GO@MOF-5 as catalyst on thermal decomposition of ammonium perchlorate, Nanoscale Res. Lett. 14 (2019), https://doi.org/10.1186/s11671-019-3163-z.
[46] M.D. Firouzjaei, A.A. Shamsabadi, M. Sharifian Gh, A. Rahimpour, M. Soroush, A novel nanocomposite with superior antibacterial activity: a silver-based metal organic framework embellished with graphene oxide, Adv. Mater. Interfaces 5 (2018), 1701365, https://doi.org/10.1002/admi.201701365.
[47] I.R. Indran, G. Tufo, S. Pervaiz, C. Brenner, Recent advances in apoptosis, mitochondria and drug resistance in cancer cells, Biochim. Biophys. Acta, Bioenerg. 1807 (2011) 735–745.
[48] C.M. Pfeffer, A.T.K. Singh, Apoptosis: a target for anticancer therapy, Int. J. Mol. Sci. 19 (2018), https://doi.org/10.3390/ijms19020448.
[49] D.M. Valcourt, J. Harris, R.S. Riley, M. Dang, J. Wang, E.S. Day, Advances in targeted nanotherapeutics: from bioconjugation to biomimicry, Nano Res. 11 (2018) 4999–5016, https://doi.org/10.1007/s12274-018-2083-z.
[50] T.A. Debele, C. Yeh, W. Su, in: Cancer Immunotherapy and Application of Nanoparticles in Cancers Immunotherapy as the Delivery of Immunotherapeutic Agents and as the Immunomodulators, 2020, pp. 1–24.
[51] L. Smith, Z. Kuncic, K. Ostrikov, S. Kumar, Nanoparticles in cancer imaging and therapy, J. Nanomater. 2012 (2012), https://doi.org/10.1155/2012/891318.
[52] R. Zein, W. Sharrouf, K. Selting, Physical properties of nanoparticles that result in improved cancer targeting, J. Oncol. 2020 (2020), https://doi.org/10.1155/2020/5194780.
[53] M.D. Firouzjaei, M. Pejman, M.S. Gh, S.A. Aktij, E. Zolghadr, A. Rahimpour, M. Sadrzadeh, A.A. Shamsabadi, A. Tiraferri, M. Elliott, Functionalized polyamide membranes yield suppression of biofilm and planktonic bacteria while retaining flux and selectivity, Sep. Purif. Technol. 282 (2021), 119981.
[54] M. Pejman, M.D. Firouzjaei, S.A. Aktij, P. Das, E. Zolghadr, H. Jafarian, A. A. Shamsabadi, M. Elliott, M.R. Esfahani, M. Sangermano, Improved antifouling and antibacterial properties of forward osmosis membranes through surface modification with zwitterions and silver-based metal organic frameworks, J. Membr. Sci. 611 (2020), 118352.
[55] M.D. Firouzjaei, A.A. Shamsabadi, M.S. Gh, A. Rahimpour, M. Soroush, A novel nanocomposite with superior antibacterial activity: a silver-based metal organic framework embellished with graphene oxide, Adv. Mater. Interfaces 5 (2018).
[56] M. Pejman, M.D. Firouzjaei, S.A. Aktij, E. Zolghadr, P. Das, M. Elliott, M. Sadrzadeh, M. Sangermano, A. Rahimpour, A. Tiraferri, Effective strategy for UV-mediated grafting of biocidal ag-MOFs on polymeric membranes aimed at enhanced water ultrafiltration, Chem. Eng. J. 426 (2021), 130704.
[57] S.F. Seyedpour, M. Dadashi Firouzjaei, A. Rahimpour, E. Zolghadr, A. Arabi Shamsabadi, P. Das, F. Akbari Afkhami, M. Sadrzadeh, A. Tiraferri, M.A. Elliott, Toward sustainable tackling of biofouling implications and improved performance of TFC FO membranes modified by Ag-MOFs nanorods, ACS Appl. Mater. Interfaces 12 (2020) 38285–38298.
[58] D. Santjojo, M.A. Abdillah, M.C. Padaga, S.P. Sakti, Effect of electron density and temperature in oxygen plasma treatment of polystyrene surface, in: IOP Conf. Ser. Mater. Sci. Eng, IOP Publishing, 2019, p. 12061.
[59] M. Pejman, M. Dadashi Firouzjaei, S. Aghapour Aktij, P. Das, E. Zolghadr, H. Jafarian, A. Arabi Shamsabadi, M. Elliott, M. Sadrzadeh, M. Sangermano, In situ Ag-MOF growth on pre-grafted zwitterions imparts outstanding antifouling properties to forward osmosis membranes, ACS Appl. Mater. Interfaces 12 (2020) 36287–36300.

[60] B.-T. Qu, J.-C. Lai, S. Liu, F. Liu, Y.-D. Gao, X.-Z. You, Cu-and ag-based metal-organic frameworks with 4-Pyranone-2, 6-dicarboxylic acid: syntheses, crystal structures, and dielectric properties, Cryst. Growth Des. 15 (2015) 1707–1713.
[61] X. Zhou, Y. Zhang, Z. Huang, D. Lu, A. Zhu, G. Shi, Ionic liquids modified graphene oxide composites: a high efficient adsorbent for phthalates from aqueous solution, Sci. Rep. 6 (2016), srep38417.
[62] C. Tao, J. Wang, S. Qin, Y. Lv, Y. Long, H. Zhu, Z. Jiang, Fabrication of pH-sensitive graphene oxide–drug supramolecular hydrogels as controlled release systems, J. Mater. Chem. 22 (2012) 24856–24861.
[63] S. Frindy, A. Primo, H. Ennajih, A. el Kacem Qaiss, R. Bouhfid, M. Lahcini, E. M. Essassi, H. Garcia, A. El Kadib, Chitosan–graphene oxide films and CO 2-dried porous aerogel microspheres: interfacial interplay and stability, Carbohydr. Polym. 167 (2017) 297–305.
[64] S. Pei, H.-M. Cheng, The reduction of graphene oxide, Carbon N. Y. 50 (2012) 3210–3228.
[65] A.M. Ferraria, A.P. Carapeto, A.M.B. do Rego, X-ray photoelectron spectroscopy: silver salts revisited, Vacuum 86 (2012) 1988–1991.
[66] Y. Ouyang, X. Cai, Q. Shi, L. Liu, D. Wan, S. Tan, Y. Ouyang, Poly-l-lysine-modified reduced graphene oxide stabilizes the copper nanoparticles with higher water-solubility and long-term additively antibacterial activity, Colloids Surf. B: Biointerfaces 107 (2013) 107–114.
[67] A.F. de Faria, A.C.M. de Moraes, P.D. Marcato, D.S.T. Martinez, N. Durán, A. G. Souza Filho, A. Brandelli, O.L. Alves, Eco-friendly decoration of graphene oxide with biogenic silver nanoparticles: antibacterial and antibiofilm activity, J. Nanopart. Res. 16 (2014) 2110.
[68] C. Deetuam, C. Samthong, S. Thongyai, P. Praserthdam, A. Somwangthanaroj, Synthesis of well dispersed graphene in conjugated poly (3, 4-ethylenedioxythiophene): polystyrene sulfonate via click chemistry, Compos. Sci. Technol. 93 (2014) 1–8.
[69] J. Tang, Q. Chen, L. Xu, S. Zhang, L. Feng, L. Cheng, H. Xu, Z. Liu, R. Peng, Graphene oxide–silver nanocomposite as a highly effective antibacterial agent with species-specific mechanisms, ACS Appl. Mater. Interfaces 5 (2013) 3867–3874.
[70] C. Berrouet, N. Dorilas, K.A. Rejniak, N. Tuncer, Comparison of Drug Inhibitory Effects ($$\hbox IC _ 50 $$ IC 50) in Monolayer and Spheroid Cultures, Bull. Math. Biol. 82 (2020) 1–23.
[71] E. Ploetz, A. Zimpel, V. Cauda, D. Bauer, D.C. Lamb, C. Haisch, S. Zahler, A. M. Vollmar, S. Wuttke, H. Engelke, Metal-organic framework nanoparticles induce pyroptosis in cells controlled by the extracellular pH, Adv. Mater. 32 (2020) 1907267.
[72] L. Liu, J. Liu, Y. Wang, X. Yan, D.D. Sun, Facile synthesis of monodispersed silver nanoparticles on graphene oxide sheets with enhanced antibacterial activity, New J. Chem. 35 (2011) 1418–1423.
[73] D. McShan, P.C. Ray, H. Yu, Molecular toxicity mechanism of nanosilver, J. Food Drug Anal. 22 (2014) 116–127, https://doi.org/10.1016/j.jfda.2014.01.010.
[74] F. Faedmaleki, F.H. Shirazi, A.A. Salarian, H.A. Ashtiani, H. Rastegar, Toxicity effect of silver nanoparticles on mice liver primary cell culture and HepG2 cell line, Iran. J. Pharm. Res. 13 (2014) 235–242, https://doi.org/10.22037/ijpr.2014.1436.
[75] A.C. Gomathi, S.R. Xavier Rajarathinam, A. Mohammed Sadiq, S. Rajeshkumar, Anticancer activity of silver nanoparticles synthesized using aqueous fruit shell extract of Tamarindus indica on MCF-7 human breast cancer cell line, J. Drug Deliv Sci. Technol. 55 (2020), 101376, https://doi.org/10.1016/j.jddst.2019.101376.
[76] K. Satyavani, S. Gurudeeban, T. Ramanathan, T. Balasubramanian, Toxicity study of silver nanoparticles synthesized from Suaeda monoica on Hep-2 cell line, Avicenna J. Med. Biotechnol. 4 (2012) 35–39.
[77] L. Ou, B. Song, H. Liang, J. Liu, X. Feng, B. Deng, T. Sun, L. Shao, Toxicity of graphene-family nanoparticles: a general review of the origins and mechanisms, Part. Fibre Toxicol. 13 (2016), https://doi.org/10.1186/s12989-016-0168-y.
[78] T.A. Tabish, M.Z.I. Pranjol, F. Jabeen, T. Abdullah, A. Latif, A. Khalid, M. Ali, H. Hayat, P.G. Winyard, J.L. Whatmore, S. Zhang, Investigation into the toxic effects of graphene nanopores on lung cancer cells and biological tissues, Appl. Mater. Today 12 (2018) 389–401, https://doi.org/10.1016/j.apmt.2018.07.005.
[79] Z. Tang, L. Zhao, Z. Yang, Z. Liu, J. Gu, B. Bai, J. Liu, J. Xu, H. Yang, Mechanisms of oxidative stress, apoptosis, and autophagy involved in graphene oxide nanomaterial anti-osteosarcoma effect, Int. J. Nanomedicine 13 (2018) 2907–2919, https://doi.org/10.2147/IJN.S159388.
[80] E.L. Gregoraszczuk, A. Rak-Mardyła, J. Ryś, J. Jakubowicz, K. Urbański, Effect of chemotherapeutic drugs on Caspase-3 activity, as a key biomarker for apoptosis in ovarian tumor cell cultured as monolayer. A pilot study, Iran. J. Pharm. Res. 14 (2015) 1153–1161, https://doi.org/10.22037/ijpr.2015.1726.
[81] S. Arora, J. Jain, J.M. Rajwade, K.M. Paknikar, Cellular responses induced by silver nanoparticles: in vitro studies, Toxicol. Lett. 179 (2008) 93–100, https://doi.org/10.1016/j.toxlet.2008.04.009.
[82] S.W. Wang, C.H. Lee, M.S. Lin, C.W. Chi, Y.J. Chen, G.S. Wang, K.W. Liao, L. P. Chiu, S.H. Wu, D.M. Huang, L. Chen, Y.S. Shen, ZnO nanoparticles induced caspase-dependent apoptosis in gingival squamous cell carcinoma through mitochondrial dysfunction and p70s6K signaling pathway, Int. J. Mol. Sci. 21 (2020) 1–16, https://doi.org/10.3390/ijms21051612.
[83] I. Ullah, A.T. Khalil, M. Ali, J. Iqbal, W. Ali, S. Alarifi, Z.K. Shinwari, Green-synthesized silver nanoparticles induced apoptotic cell death in MCF-7 breast cancer cells by generating reactive oxygen species and activating caspase 3 and 9 enzyme activities, Oxidative Med. Cell. Longev. 2020 (2020), https://doi.org/10.1155/2020/1215395.
[84] M. Morales-Cruz, C.M. Figueroa, T. González-Robles, Y. Delgado, A. Molina, J. Méndez, M. Morales, K. Griebenow, Activation of caspase-dependent apoptosis by intracellular delivery of cytochrome c-based nanoparticles, J. Nanobiotechnol. 12 (2014) 1–11, https://doi.org/10.1186/s12951-014-0033-9.
[85] S. Lin, J. Lv, P. Peng, C. Cai, J. Deng, H. Deng, X. Li, X. Tang, Bufadienolides induce p53-mediated apoptosis in esophageal squamous cell carcinoma cells in vitro and in vivo, Oncol. Lett. 15 (2018) 1566–1572.
[86] M. Burnett, Y. Abuetabh, A. Wronski, F. Shen, S. Persad, R. Leng, D. Eisenstat, C. Sergi, Graphene oxide nanoparticles induce apoptosis in wild-type and CRISPR/Cas9-IGF/IGFBP3 knocked-out osteosarcoma cells, J. Cancer 11 (2020) 5007–5023, https://doi.org/10.7150/jca.46464.
[87] L.D. Walensky, Targeting BAX to drug death directly, Nat. Chem. Biol. 15 (2019) 657–665.
[88] X. Zhang, X. Liu, D. Zhou, G. Zheng, Targeting Anti-apoptotic BCL-2 Family Proteins for Cancer Treatment, 2020.
[89] J.M. Wang, B.L. Xiao, J.W. Zheng, H.B. Chen, S.Q. Zou, Effect of targeted magnetic nanoparticles containing 5-FU on expression of bcl-2, bax and caspase 3 in nude mice with transplanted human liver cancer, World J. Gastroenterol. 13 (2007) 3171–3175, https://doi.org/10.3748/wjg.v13.i23.3171.
[90] S. Alarifi, H. Ali, S. Alkahtani, M.S. Alessia, Regulation of apoptosis through bcl-2/bax proteins expression and DNA damage by nano-sized gadolinium oxide, Int. J. Nanomedicine 12 (2017) 4541–4551, https://doi.org/10.2147/IJN.S139326.
[91] N. Khan, H. Mukhtar, in: 14.20 Cancer Chemoprevention, 2010, p. 12.
[92] J.E. Chipuk, D.R. Green, How do BCL-2 proteins induce mitochondrial outer membrane permeabilization? Trends Cell Biol. 18 (2008) 157–164, https://doi.org/10.1016/j.tcb.2008.01.007.
[93] A.E. El-Sisi, S.S. Sokkar, H.A. Ibrahim, M.F. Hamed, S.E. Abu-Risha, Targeting MDR-1 gene expression, BAX/BCL2, caspase-3, and Ki-67 by nanoencapsulated imatinib and hesperidin to enhance anticancer activity and ameliorate cardiotoxicity, Fundam. Clin. Pharmacol. 34 (2020) 458–475.